Hydrodynamical modelling of Type IIb SNe.

M. Ergon[1], F. Taddia[1], M. Stritzinger[2], A. Jerkstrand[3], J, Sollerman[1], and C. Fransson[1]

[1] The Oskar Klein Centre, Department of Astronomy, AlbaNova, Stockholm University, 106 91 Stockholm, Sweden
[2] Department of Physics and Astronomy, Aarhus University, Ny Munkegade 120, 8000 Aarhus C, Denmark
[3] Astrophysics Research Center, School of Mathematics and Physics, Queens University Belfast, Belfast, BT7 1NN, UK
[4] Kavli Institute for the Physics and Mathematics of the Universe, Todai Institutes for Advanced Study, University of Tokyo, 5-1-5 Kashiwanoha, Kashiwa, Chiba 277-8583, Japan

ABSTRACT

We use HYDE, a new one-dimensional hydrodynamical code, to construct a grid of supernova (SN) models based on solar metallicity bare helium core models evolved to the verge of core-collapse with MESA STAR. This grid is well suited to model Type IIb SNe, which progenitor stars are thought to have lost all but a tiny fraction of their hydrogen envelopes. As previously demonstrated such an envelope only affects the early lightcurve, and the diffusion phase and the early tail phase lightcurves are determined by the helium core. Relatively massive hydrogen envelopes do affect the photospheric velocities during the diffusion phase, however, which could lead to underestimates of the explosion energy. Using an automated procedure we fit the bolometric lightcurves and photospheric velocities of the Carnegie Supernova Project (CSP) and literature samples of Type IIb SNe to the grid of SN models. We find the distribution of initial masses for the combined sample, consisting of Type 17 IIb SNe, to be reasonably well described by a standard Salpeter IMF. The fraction of SNe with an initial mass <15 $M_\odot$ and <20 $M_\odot$ is 50 and 88 percent, respectively, suggesting either the binary channel to dominate the the production of Type IIb SNe or a significant revision of stellar mass loss rates. We find correlations between the explosion energy, initial mass and mass of ^{56}Ni, the explosion energy increasing with initial mass and the mass of ^{56}Ni increasing with explosion energy. The method used allows us to determine the errors in the model parameters arising from the observed quantities and the degeneracy of the solution. We find an error in the distance and extinction to propagate mainly to the derived mass of ^{56}Ni, whereas an error in the photospheric velocity propagates mainly to the derived helium core mass and explosion energy. Fits using the bolometric lightcurve alone are completely degenerate along the M_{ej}^2/E=const curve, whereas fits using also the photospheric velocities are quite robust for well-sampled SNe. Finally, we provide a description of the HYDE code, tests and a discussion of its limitations.

Key words. supernovae: general — supernovae: individual (SN 2011dh) — galaxies: individual (M51)

1. Introduction

Type IIb supernovae (SNe) are thought to arise from stars that have lost most of their hydrogen envelopes, either through stellar winds or through Roche-lobe overflow to a binary companion. These SNe are observationally characterized by a transition from Type II (with a hydrogen signature) to Type Ib (without a hydrogen but with a helium signature). Whether binary or single progenitor systems are dominating the production of Type IIb SNe is still debated, but for SN 1993J a companion star have been detected by direct observations (Maund et al. 2004; Fox et al. 2014). Because most of the hydrogen envelope have been lost, whereas the helium core is still intact, we expect these SNe to be well approximated by the explosion of bare helium cores, except during the early cooling phase. This method have been used by Bersten et al. (2012), and allows for estimates of the helium core mass, explosion energy and mass of ^{56}Ni, whereas the progenitor radius can not be estimated without taking the hydrogen envelope into account. Type IIb SNe have the unique quality to allow an estimate of the helium core mass which, contrary to the ejecta mass, is directly linked to the initial mass of the star. Some parameter studies have been published (e.g. Lyman et al. 2014), but are all based on approximate lightcurve modelling (e.g. Arnett 1982). The aim of this paper is to use the new hydrodynamical code HYDE to construct a grid of SN mod-

els based on bare helium core models, and use this to estimate the progenitor and SN parameters for the Carnegie Supernova Project (CSP) and literature samples of Type IIb SNe.

Application of hydrodynamics to SNe lightcurves was introduced in the 70:ths (e.g. Falk & Arnett 1977), and since then a number of codes spanning a wide range of complexity have followed. Some implements more advanced physics, as multi-dimensional (e.g. Mueller et al. 1991) and radiation (e.g. Blinnikov et al. 1998) hydrodynamics, whereas others are one-dimensional and based on the diffusion approximation (e.g. Bersten et al. 2011). The different codes all have their different applications and no code is yet capable of modelling a core-collapse (CC) SN consistently, including all the relevant physics. HYDE belongs to the latter category, and like other simplified codes it have the benefit of being fast, which is critical when building model grids covering large volumes of parameter space. The use of model grids to determine the SN and progenitor parameters have been explored before (e.g. Litvinova & Nadezhin 1983, 1985) with somewhat mixed results (e.g. Hamuy 2003), but the decreasing computational cost and the increasing amount of data, motivates a renewed interest in this approach. A model grid also allows the degeneracy of the solution and the errors in the SN and progenitor parameters to be estimated.

The paper is organized as follows. In Sect. 2 we describe and test the HYDE code, and discuss its limitations. In Sect. 3

we describe the grid of bare helium core and SN models, and discuss the dependence of the observed properties on the SN and progenitor parameters. In Sect. 4 we present models with low-mass hydrogen envelopes, and discuss the effects of these on the observed properties. In Sect. 5 we describe our fitting procedure, use the grid of SN models to estimate the progenitor and SN parameters for the CSP and literature samples of Type IIb SNe, and discuss the total sample statistics. The observational details for the CSP and literature samples are given in Appendices A and B, respectively. Finally, we conclude and summarize the paper in Sect. 6.

2. The HYDE code

HYDE is a one-dimensional Lagrangian hydrodynamical code based on the flux-limited diffusion approximation, following the method described in Falk & Arnett (1977). The code may also be run in homologous mode, where the dynamics have been switched off and the thermodynamical state is solved for given the constraint of homologous expansion.

2.1. Hydrodynamics

The hydrodynamical conservation equations for mass, momentum and energy coupled with the diffusion approximation (Falk & Arnett 1977, eqs. 1-4) are solved by a finite difference scheme similar to the one described by Falk & Arnett (1977, eqs. A1-A12). The dynamical state is solved for using a forward difference scheme, whereas the thermodynamical state is solved for using a backward difference scheme. The latter results in a non-linear equation system which is solved using a Newton-Raphson like method. To handle strong velocity gradients (shocks) an artificial viscosity following the prescription by Von Neumann & Richtmyer (1950) is used, and in the optically thin regime a flux limiter following the prescription given by Bersten et al. (2011) is used.

2.2. Opacity

The opacity is interpolated from the OPAL opacity tables (Iglesias & Rogers 1996) complemented with the low temperature opacities given by Alexander & Ferguson (1994). In addition we use an opacity floor set to 0.01 cm^2 $gram^{-1}$ in the hydrogen envelope and 0.025 cm^2 $gram^{-1}$ in the helium core, following Bersten et al. (2012, private communication), who calibrated these values by comparison to the STELLA hydrodynamical code (Blinnikov et al. 1998).

2.3. Equation of state

The equation of state is taken to be that of a mixture of gas and radiation, and degeneracy pressure is not included. The electron density needed in the equation of state is calculated by solving the Saha equation, using the same atomic data as in Jerkstrand et al. (2011, 2012).

2.4. Radioactive heating

The transfer of the gamma-rays and positrons emitted in the decay chain of ^{56}Ni is calculated with a Monte-Carlo method, using the same grey opacities, luminosities and decay times as in Jerkstrand et al. (2011, 2012), and the heating rate then fed into the energy equation.
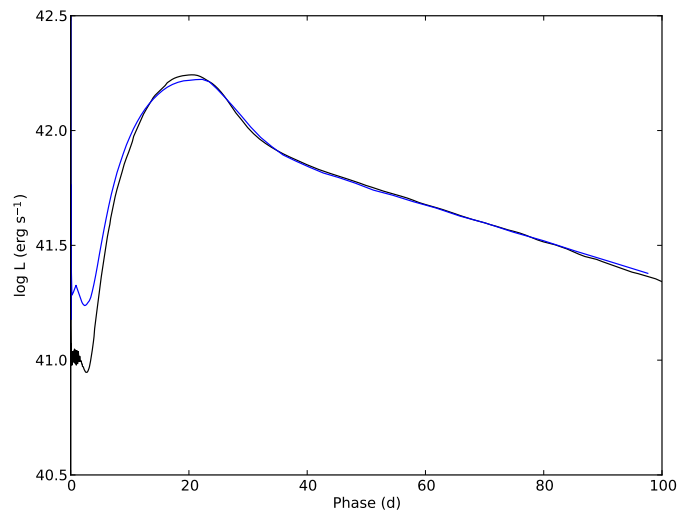
Fig. 1. Bolometric lightcurve for the 4 $M_\odot$ bare helium core model from Nomoto & Hashimoto (1988) as modelled with HYDE (black) and the adjusted version of the Bersten et al. (2012) He4 model presented in Ergon et al. (2014b) (blue).
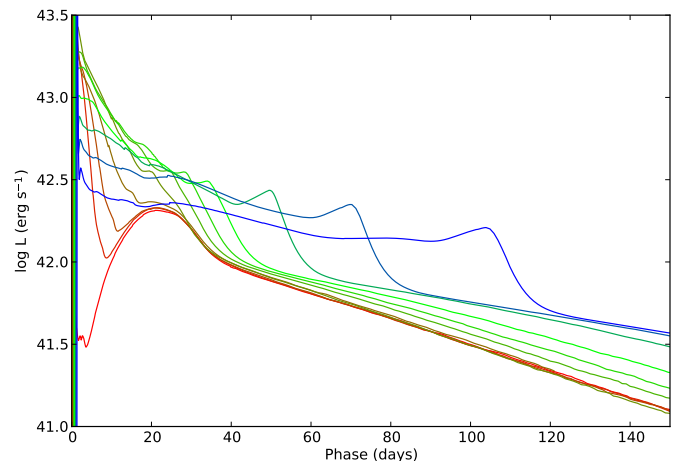

Fig. 2. Progression of model bolometric lightcurves calculated with HYDE for a 15 $M_\odot$ MESA model with the massloss adjusted to yield a final mass of 11.0, 8.0, 6.0, 5.0, 4.8, 4.6, 4.4, 4,2, 4.1, 4.05 and 4.0 $M_\odot$, colour coded from blue (11.0 $M_\odot$) to red (4.0 $M_\odot$). The explosion parameters were E=1.0×10^{51}erg, M_{Ni}=0.1 $M_\odot$ and Mix$_{Ni}$=M$_{He}$/M (Sect. 3).

2.5. Limitations

The effects of explosive nucleosynthesis are ignored as a nuclear network is not included, and macroscopic mixing is prohibited as the code is one-dimensional. The optically thin regime is not handled correctly as the code is based on the diffusion approximation, but a rough treatment is provided by the flux limiter. The table bound-bound opacity is not correctly calculated as a static medium was assumed, but a rough correction is provided by the use of opacity floor.

2.6. Tests of the code

The homologous behaviour have been tested by comparison to analytical solutions by Imshennik & Popov (1992), and the deposition of radioactive decay energy have been tested by comparison to the steady-state NLTE code described in Jerkstrand et al.

(2011, 2012). The hydrodynamical behaviour have been tested by comparison to the results presented in Bersten et al. (2012) using the same 4 $M_\odot$ bare helium core model from Nomoto & Hashimoto (1988). Figure 1 shows a comparison between the lightcurve calculated with HYDE and the lightcurve for the adjusted version of the Bersten et al. (2012) He4 model presented in Ergon et al. (2014b). Both models have the same explosion parameters (E=1.0×10^{51} erg, M_{NI}=0.075 $M_\odot$ and Mix_{Ni}=0.95). Except at $\lesssim$5 days the differences are small, but the early time luminosity is considerably lower. The reason for this difference is unclear and needs further investigation, but as we only make use of the diffusion and tail phase lightcurves in this work, we find the agreement satisfactory. Fiure 2 show lightcurves calculated with HYDE for a series of 15 $M_\odot$ MESA models were the mass-loss was adjusted to yield final masses in the range 11-4 $M_\odot$. The sequence of lightcurves shows the expected transformation from an explosion energy powered Type IIP like lightcurve to a radioactively powered Type Ib like lightcurve. Further support comes from the behaviour of observed and physical properties of bare helium core and extended models, discussed in Sects. 3.3, 3.4, 4.1 and 4.2.

3. The model grid

3.1. Progenitor models

The progenitor models were constructed using MESA STAR (Paxton et al. 2011) by evolving solar metallicity helium cores until the verge of core-collapse. This is similar to what was done in Nomoto & Hashimoto (1988), and relays on the assumption that the hydrogen envelope does not appreciably affect the evolution of the helium core. Evolving a set of solar metallicity 15 $M_\odot$ models, adjusting the mass loss to yield final masses in the range 15-4 $M_\odot$, resulted in helium cores of very similar size and composition, in support of this assumption. The MESA configuration used was the default one, and the evolution were terminated at a central density of $10^{9.5}$ g cm^{-3}, which typically occurred slightly before core-collapse. The evolved models spans M_{He}=4.0-5.0 $M_\odot$ in 0.25 $M_\odot$ steps and M_{He}=5.0-10.0 $M_\odot$ in 0.5 $M_\odot$ steps. Below 4.0 $M_\odot$ the late burning stages ignited off center, which caused convergence problems, and these stellar models were constructed by a scaling of the 4.0 $M_\odot$ density profile.

3.2. SN models

As all similar codes, HYDE does not include a treatment of the physics of the core-collapse itself. Instead the outcome of this event is simulated by the injection of thermal energy (thermal bomb) at some location assumed to correspond to the division between the collapsing core and the ejected material. This location is fixed to 1.5 $M_\odot$ in all our models, and the explosion energy (E) is treated as a free parameter. The current version of HYDE does not include a network of nuclear reactions, so the explosive nuclear burning occurring in the iron core and the inner parts of the oxygen zones, synthesizing the radioactive isotopes powering the lightcurve, can not be modelled. Because of this, and the absence of multi-dimensional effects as macroscopic mixing in 1-D (spherical symmetric) modelling, the mass (M_{Ni}) and mixing (Mix_{Ni}) of the ^{56}Ni are also treated as free parameters. The mass fraction of ^{56}Ni (X_{Ni}) was assumed to be a linearly declining function of the ejecta mass (m_{ej}) becoming zero at some fraction (Mix_{Ni}) of the total ejecta mass, expressed as $X_{Ni} \propto 1 - m_{ej}/(Mix_{Ni}M_{ej}), X_{Ni} \geq 0$. Note that this expression allows $Mix_{Ni} > 1$, although the interpretation then becomes
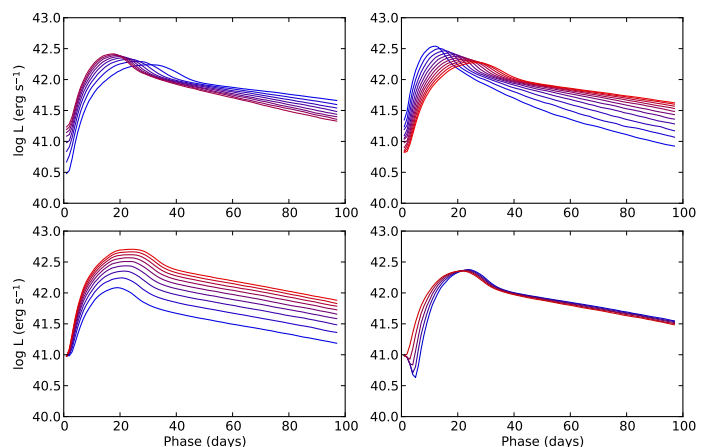

Fig. 3. Model bolometric lightcurves for day 0-100 showing the dependence on M_{He} (upper left panel), E (upper right panel), M_{Ni} (lower left panel) and Mix_{Ni} (lower right panel). Low to high values are displayed in red to blue colour coding and the values for the parameters not varied are set to M_{He}=4.0 $M_\odot$, E=1.0×10^{52} erg, M_{Ni}=0.1 $M_\odot$ and Mix_{Ni}=1.0.
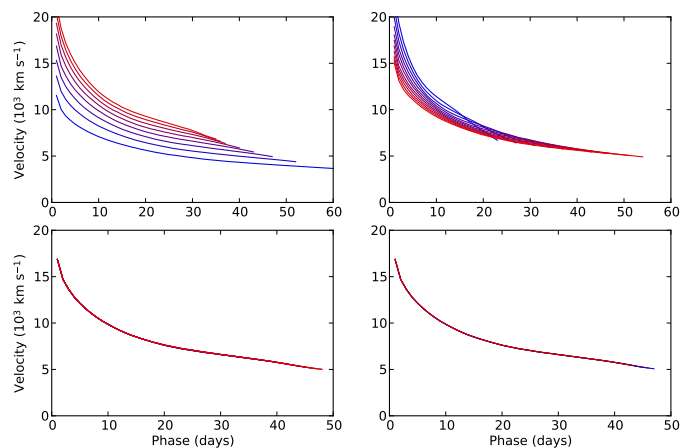

Fig. 4. Model photospheric velocities for day 0-100 showing the dependence on M_{He} (upper left panel), E (upper right panel), M_{Ni} (lower left panel) and Mix_{Ni} (lower right panel). Low to high values are displayed in red to blue colour coding and the values for the parameters not varied are set to M_{He}=4.0 $M_\odot$, E=1.0×10^{52} erg, M_{Ni}=0.1 $M_\odot$ and Mix_{Ni}=1.0.

less clear. The SN explosion is thus parametrized using three parameters (E, M_{Ni} and Mix_{Ni}) and the progenitor star using one (M_{He}). The total parameter space spanned is M_{He}=2.5-10 $M_\odot$, E=0.4-6.0×10^{51} erg, M_{Ni}=0.015-0.3 $M_\odot$ and Mix_{Ni}=0.5-1.4 using a 21×24×15×9 grid. We find this resolution to be sufficient to safely interpolate intermediate values.

3.3. Dependence on progenitor and SN parameters

Fig. 3 shows the dependence of the bolometric lightcurve on M_{He}, E, M_{Ni} and Mix_{Ni}, varying the parameters for a reference model with M_{He}=4.0 $M_\odot$, E=1.0×10^{52} erg, M_{Ni}=0.1 $M_\odot$ and Mix_{Ni}=1.0. Qualitatively, we expect either an increase of the explosion energy or a decrease of the ejecta mass to decrease the diffusion time for thermal radiation, to decrease the optical depth for the γ-rays emitted in the decay chain of ^{56}Ni, and to increase the expansion velocities. We therefore expect such a

change to decrease the time at which peak luminosity occurs, to decrease the luminosity on the tail and to decrease the photospheric velocity. Qualitatively, we also expect the luminosity to scale with the mass of ^{56}Ni. As seen in Fig. 3, all these qualitative dependencies are well followed by the models. Quantifying the dependencies by measuring the time (t_m) and photospheric velocity (v_m) at maximum luminosity (L_m) for Mix$_{Ni}$=1.0, and fitting a power-law expression to the model grid, we get

$$\log t_m = 1.17 - 0.39 \log E + 0.69 \log M_{ej} + 0.10 \log M_{Ni} \quad (1)$$

$$\log v_m = 1.05 + 0.48 \log E - 0.18 \log M_{ej} \quad (2)$$

$$\log L_m = 1.40 + 0.19 \log E - 1.38 \log M_{ej} + 0.83 \log M_{Ni} \quad (3)$$

which gives the (average) dependence of the observed quantities on the SN and progenitor parameters for the model grid. Fitting the inverse relations[1], we get

$$\log E = -3.21 + 0.53 \log t_m - 0.07 \log L_m + 2.55 \log v_m \quad (4)$$

$$\log M = -2.65 + 1.40 \log t_m - 0.17 \log L_m + 1.20 \log v_m \quad (5)$$

$$\log M_{Ni} = -5.45 + 2.23 \log t_m + 0.92 \log L_m + 1.46 \log v_m \quad (6)$$

which gives the (average) dependence of the SN and progenitor parameters on the observed quantities for the model grid. Using the observed values for SN 2011dh we get values for E, M_{ej} and M_{Ni} within ~10 percent of those derived by the fitting procedure in Sect. 5, and a clever parametrization of the model grid could actually be an alternative to this fitting procedure. However, given the dubious results obtained from the model grid fits for Type IIP SNe by Litvinova & Nadezhin (1983, 1985) in e.g. Hamuy (2003), care has to be taken, and we do not investigate this approach further in this work. The approximate model by Arnett (1982) is often used to infer the SN and progenitor parameters for stripped envelope SNe (e.g. Lyman et al. 2014). In this model the diffusion time and the expansion velocity depends on the explosion energy and ejecta mass as $t_d \propto (M^3/E)^{1/4}$ and $v \propto (E/M)^{1/2}$, and inverting these gives $E \propto t_d^2 v^3$ and $M \propto t_d^2 v$. Comparing to the model grid fits we see that these scalings are qualitatively followed, but v_m is considerably less sensitive to M_{ej}, and E is considerably less sensitive to t_m. Clearly, t_m and t_d and in particular v and v_m are not identical, but most important is likely the fact that the Arnett (1982) model assumes a constant opacity, whereas in the hydrodynamical models the (average) opacity is decreasing with time as the helium recombination front recedes through the ejecta (Sect. 3.4). An important consequence of the different scalings is that t_m is independent of the quantity $M^{2.12}/E$, whereas that t_d is independent of the quantity M^3/E in the Arnett (1982) model. This has implications for the degeneracy of the solution, as we will discuss further in Sect. 5.6.
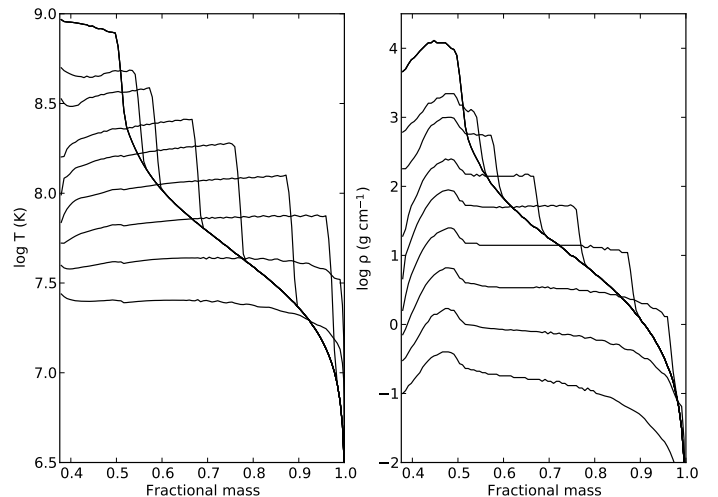
Fig. 5. Evolution of the temperature (left panel) and density (right panel) profiles between 1 and 282 seconds (shock breakout) in 10 logarithmically spaced intervals for the 4 M$_\odot$ helium core model.
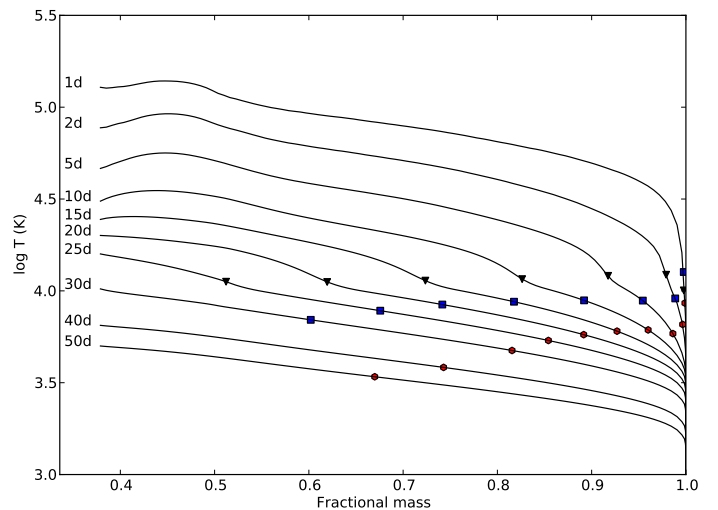

Fig. 6. Evolution of temperature profile for the 4 M$_\odot$ helium core model. The position of the recombination front of helium (black triangles), the photosphere (red circles) and the thermalization surface (blue squares) have been marked, and each temperature profile annotated with the time since explosion.

3.4. Model physics

Here we discuss the physics of our bare helium core models, exemplified by a 4 M$_\odot$ model with explosion parameters E=1.0×10^{51}erg, M$_{Ni}$=0.1 M$_\odot$ and Mix$_{Ni}$=1.0. We stress that the early evolution differ from that of an extended progenitor, which is discussed in Sect. 4.2.

Fig. 5 shows the evolution of the density and temperature profiles from the injection of explosion energy until shock breakout, which occurs at ~300 seconds. The shock initially accelerates to a speed of ~10000 km s^{-1} in the oxygen core, but decelerates to ~6000 km s^{-1} in the helium envelope, where the density gradient is small. In the outermost layers the density gradient increases drastically before it levels out in the thin convective envelope, and the shock accelerates to a speed of ~30000 km s^{-1} at shock breakout. The thermal and kinetic energy behind the

---

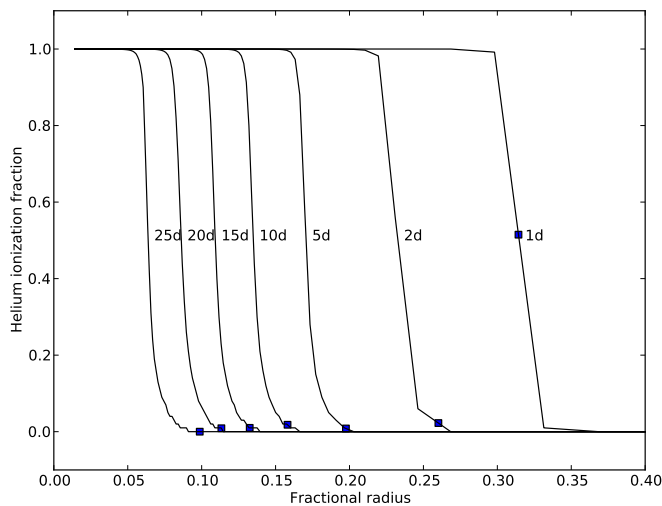[1] Note that the observed quantities are not necessarily independent.

Fig. 7. Evolution of the helium ionization profile the 4 M$_\odot$ helium core model. The thermalization surface (blue squares) have been marked and each ionization profile annotated with the time since explosion.

Fig. 8. Progression of model bolometric lightcurves calculated with HYDE for a 15 M$_\odot$ MESA model with the massloss adjusted to yield a final mass of 4.2, 4.15, 4.1, 4.05, 4.025 and 4.0 M$_\odot$, colour coded from blue (4.2 M$_\odot$) to red (4.0 M$_\odot$). The explosion parameters were E=1.0×10^{51}erg, M$_{Ni}$=0.1 M$_\odot$ and Mix$_{Ni}$=M$_{He}$/M.

shock is close to equipartition and the temperature high enough for the equation of state to be completely radiation dominated. During the passage of the shock through the star some thermal energy is lost due to expansion, in particular during the passage through the thin envelope, and when the radiation breaks out from the shock the thermal fraction of the energy is ∼15 percent.

In the few minutes that follows the ejecta expands and the temperature and luminosity at the photosphere decrease rapidly because of diffusion and expansion cooling. At ∼500 seconds the outermost parts becomes optically thin and the photosphere starts to recede into the ejecta. At ∼3 hours helium starts to recombine and at ∼10 hours the recombination front overruns the photosphere. Subsequently the position of the photosphere is determined by the recombination front, slowly moving inwards in mass coordinates but outwards in radial coordinates. Fig. 6 shows the evolution of the temperature and the helium ionization profile between 1 and 50 and 1 and 25 days, respectively, where we have also marked the positions of the photosphere, the thermalization surface and the recombination front. The thermalization surface, here defined as $\sqrt{3\tau_{abs}\tau_{tot}} = 2/3$ (Ensman & Burrows 1992), is located near the outer edge of the recombination front, and follows the evolution of this until ∼25 days when the helium has recombined. During this period the temperature at the thermalization surface is roughly constant, and declines only slowly from ∼9000 K to ∼8000 K, a few thousand degrees below the temperature at the center of the recombination front.

4. The hydrogen envelope

As our aim is to use the grid of bare helium core models to fit the bolometric lightcurves and the photospheric velocities of Type IIb SNe, which may have extended low-mass hydrogen envelopes surrounding their helium cores, it is of importance to investigate which effect such envelopes would have on the observed properties. It is also of interest to investigate the physics of such models and compare to the physics of bare helium core models discussed in Sect. 3.4.
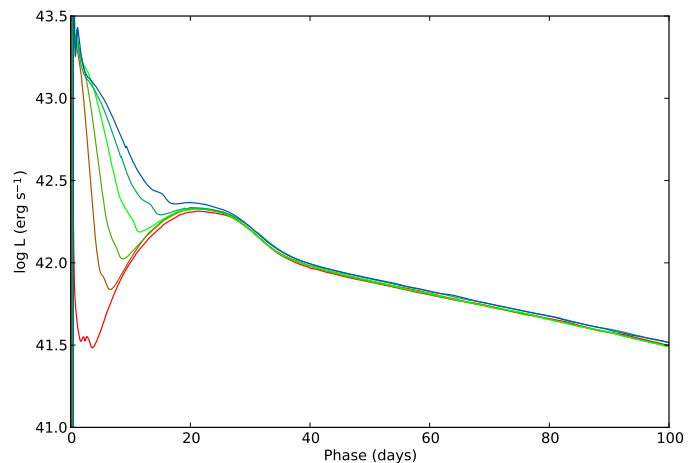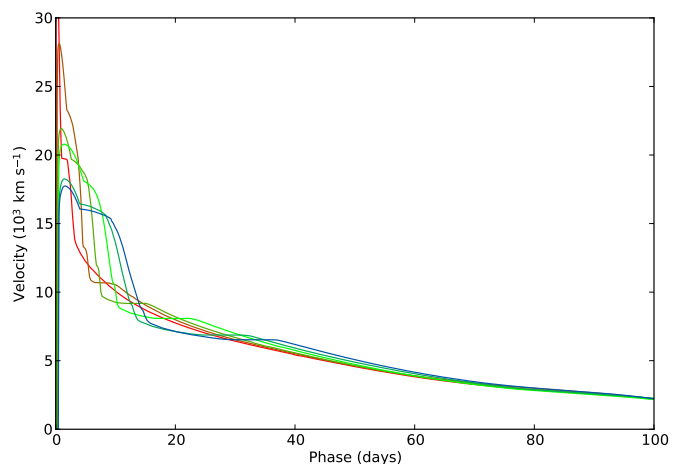
Fig. 9. Progression of model photospheric velocities calculated with HYDE for a 15 M$_\odot$ MESA model with the massloss adjusted to yield a final mass of 4.2, 4.15, 4.1, 4.05, 4.025 and 4.0 M$_\odot$, colour coded from blue (4.2 M$_\odot$) to red (4.0 M$_\odot$). The explosion parameters were E=1.0×10^{51}erg, M$_{Ni}$=0.1 M$_\odot$ and Mix$_{Ni}$=M$_{He}$/M.

4.1. Effect on the observed properties

Figs. 8 and 9 shows the bolometric lightcurve and photospheric velocities for a sequence of 15 M$_\odot$ MESA models, where the mass loss was adjusted to yield final masses in the range 4.2-4.0 M$_\odot$. Defining the hydrogen envelope to begin where X>0.01, this corresponds to hydrogen envelope masses in the range 0.27-0.07 M$_\odot$. The bolometric lightcurves for all models show an initial decline phase corresponding to the cooling of the thermal explosion energy deposited in the hydrogen envelope, the length of which decreases with decreasing mass of the envelope. The reason for this is twofold, first the thermal energy deposited in the hydrogen envelope decrease with the mass of it, and secondly the radius of the progenitor stars decrease, decreasing the time scale for expansion cooling. Models for Type IIb SNe often have an increased helium abundance in the hydrogen envelope (e.g. Woosley et al. 1994), because of mixing of helium into the base of the hydrogen envelope. This results in smaller pro-

genitor radii due to decreased opacities, and therefore in shorter durations of the cooling phase. Our models have lower helium abundances as compared Woosley et al. (1994) and Shigeyama et al. (1994), which should be kept in mind. During most of the cooling phase the photospheric velocities are much higher than those for a bare helium core model, but decrease quickly at the luminosity minimum, after which follow a period when they are significantly lower. The latter effect is larger for models with more massive hydrogen envelopes and is likely caused by deceleration of the helium core. As suggested by the dependencies on the photospheric velocity discussed in Sect. 3.3 and as demonstrated in Sect. 5.5, the sensitivity of the estimated explosion energy to an error in the photospheric velocity is high ($E \sim v^3$), whereas the sensitivity of the helium core mass is lower ($M_{He} \sim v$). Therefore the presence of a relatively massive hydrogen envelope could have a significant effect on the estimated explosion energy when using bare helium core models. Otherwise, the presence of the hydrogen envelope does not seem to appreciably affect the observed properties after the luminosity minimum.

4.2. Model physics

Here we discuss the physics of models with low-mass hydrogen envelopes, exemplified by the 4.05 $M_\odot$ model shown in Figs. 8 and 9. This model have an hydrogen envelope of 0.17 $M_\odot$, an average hydrogen fraction in the envelope of 0.5, and reach the luminosity minimum at ~11 days, which is similar to, but slightly later than was observed for SN 1993J.

The passage of the shock through the helium core proceeds as described for the bare helium core model, and in the steep density gradient between the helium core and the hydrogen envelope it accelerates to ~20000 km s^{-1}. Once in the hydrogen envelope, where the density is roughly constant, the shock gradually decelerates to ~6000 km s^{-1}, which give rise to a reverse shock propagating backwards into the helium envelope. During the passage of the shock through the hydrogen envelope, the helium core expands and most of the deposited thermal energy is cooled away. At shock breakout the (relatively) cool and expanded helium core is surrounded by the hot and compressed hydrogen envelope, and the subsequent evolution is determined by the expansion and cooling of this envelope. The fraction of the energy deposited in the envelope is about 10 percent, roughly equipartioned into thermal and kinetic energy.

Fig. 10 shows the evolution of the density and temperature profiles from shock breakout, which occurs at ~0.3 days, until the luminosity minimum. The profiles are similar to those obtained by modelling of SN 1993J in Woosley et al. (1994), Shigeyama et al. (1994) and Blinnikov et al. (1998). Initially the hydrogen envelope is opaque and ionized, and the surface luminosity and temperature decreasing by expansion cooling, but at ~4 days the outer parts become optically thin and the photosphere starts to recede into the ejecta. The helium starts to recombine at about the same time, whereas hydrogen stays ionized until ~7 days, and at about ~6 days the photosphere starts to trace the helium recombination front as in the bare helium core models. At the luminosity minimum the hydrogen in the envelope has recombined, the photosphere is located close to the interface between the hydrogen and helium envelope, and the temperature at the thermalization surface is ~9500 K.

5. Model grid fits

Here we use an automated procedure to fit the bolometric lightcurves and photospheric velocities for the CSP and litera-
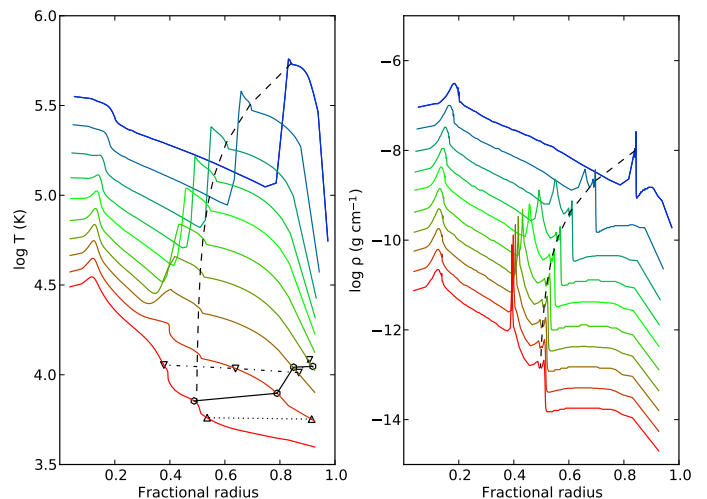

Fig. 10. Evolution of the temperature (left panel) and density (right panel) profiles betwen shock breakout and the luminosity minimum in 10 logarithmically spaced intervals for the 4.05 $M_\odot$ MESA model. The interface between the helium and hydrogen envelopes (dashed line), the photosphere (circles and dashed line) and the helium (downward triangles and dot-dashed line) and hydrogen (upward triangles and dotted line) ionization fronts are also shown.

ture samples of Type IIb SNe to those of our grid of SN models. Our method allows us to determine the sensitivity of the derived quantities to errors in the observed quantities, as well as to investigate the degeneracy of the solutions found. As discussed the grid is based on bare helium core models, and given the influence of a low-mass hydrogen envelope on the observed properties (Sect. 4.1), the diffusion phase and early tail lightcurves and the diffusion phase photospheric velocities are used to determine the SN and helium core parameters. We also make the assumption, justified for Type IIb SNe, that the helium core is not affected by mass loss. The hydrogen envelope only affects the bolometric lightcurve in the cooling phase, and the parameters of this envelope has to be modelled separately. However, relatively massive hydrogen envelopes do affect the photospheric velocities in the diffusion phase, which might lead to significant underestimates of the explosion energy (Sect. 4.1).

5.1. The CSP and literature samples

The Type IIb SNe in the CSP sample consists of SNe 2004ex, 2004ff, 2005Q, 2006T, 2006ba, 2006bf, 2008aq, 2009K, 2009Z and 2009dq (Taddia et al. 2014), of which SNe 2006bf and 2009dq have been excluded due to bad sampling of the lightcurves. The Type IIb SNe in the literature sample consists of SNe 1993J (e.g. Richmond et al. 1994, 1996), 1996cb (Qiu et al. 1999), 2003bg (Hamuy et al. 2009), 2008ax (e.g. Taubenberger et al. 2011), 2011dh (e.g. Ergon et al. 2014b), 2011fu (Kumar et al. 2013), 2011hs (Bufano et al. 2014), 2011ei (Milisavljevic et al. 2013) and 2013df (Van Dyk et al. 2014). Out of these SNe 1993J, 2008ax and 2011dh stands out by the quality of the data as well as the hard constraints on the explosion epochs. The details of the observations, the constraints on the explosion epochs and the adopted distances and extincions for the CSP and literature samples are given in Appendices A and B, respectively, where we also describe how the photospheric velocities were estimated. The pseudo-bolometric lightcurves were calculated from the photometry using the methods described in E14a, and a

UV to MIR bolometric correction determined from SN 2011dh applied. The flux falling outside this wavelength range was not corrected for, but given the results from the steady-state NLTE modelling of SN 2011dh presented in Ergon et al. (2014a), this correction is likely to be small (<0.15 mag).

5.2. Fitting procedure

The fitting is done by minimization of the square of the relative residuals, giving equal weight to the diffusion phase lightcurve, the tail lightcurve and the diffusion phase photospheric velocity evolution. The division between the diffusion and tail phases is made roughly at the point where the decline rate of the bolometric lightcurve becomes constant. If there is any sign of a cooling phase, the start of the diffusion phase is set to a few days after the rise to peak begins, and otherwise to the first observation. Photospheric velocities above the interface between the helium core and the hydrogen envelope are excluded from the fit. As discussed in E14a this velocity can be estimated from the minimum velocity for the Hα absorption minimum, but is otherwise set to 10000 km s^{-1}. As the explosion epochs in many cases are not well constrained we fit, not only the SN and progenitor parameters (M_{He}, E, M_{Ni} and Mix_{Ni}), but also the epoch of explosion, which is allowed to vary between the hard limits obtained from detections and non-detections. The errors in the bolometric lightcurves arising from the uncertainties in distance and extinction, and a systematic error in the photospheric velocities, assumed to be 15 percent, were propagated by standard methods.

5.3. Results for the CSP sample

Figure 11 shows the best-fit model bolometric lightcurve and photospheric velocity evolution compared to the (estimated) observed UV to MIR pseudo-bolometric lightcurve and estimated photosphere velocity evolution for the CSP sample of Type IIb SNe. Table 1 gives the helium core mass, explosion energy, mass and mixing of ^{56}Ni, and explosion epoch for the best-fit models and the corresponding errors. Below we review the results and compare to other results obtained in the literature.

SN 2004ex The bolometric lightcurve and photospheric velocity evolution of SN 2004ex is best fit with M_{He}=3.6 M$_\odot$, E=0.65×10^{51} erg and M_{Ni}=0.13 M$_\odot$. The fits to the bolometric lightcurve and the photospheric velocity evolution are both quite good and the solution is well constrained in the E-M_{He} plane.

SN 2004ff The bolometric lightcurve and photospheric velocity evolution of SN 2004ff is best fit with M_{He}=4.6 M$_\odot$, E=1.6×10^{51} erg and M_{Ni}=0.11 M$_\odot$. The fits to the bolometric lightcurve and the photospheric velocity evolution are both quite good and the solution is well constrained in the E-M_{He} plane. Lyman et al. (2014) found M_{ej}=1.8 M$_\odot$, E=2.9×10^{51} erg and M_{Ni}=0.22 M$_\odot$ using a fit to approximate Arnett (1982) models. Within error bars this is consistent with our results except for M_{Ni}, which could be explained by differences in the extinction and the explosion epoch.

SN 2005Q The bolometric lightcurve and photospheric velocity evolution of SN 2005Q is best fit with M_{He}=4.5 M$_\odot$, E=1.1×10^{51} erg and M_{Ni}=0.18 M$_\odot$. The fit to the bolometric lightcurve is quite good whereas the fit to the photospheric ve-

locity evolution is worse. Due to the limited rise to peak and tail coverage the constraint from the bolometric lightcurve is weak and the solution is quite degenerate along the M/E=const curve.

SN 2006T The bolometric lightcurve and photospheric velocity evolution of SN 2006T is best fit with M_{He}=3.7 M$_\odot$, E=0.70×10^{51} erg and M_{Ni}=0.075 M$_\odot$. The fits to the bolometric lightcurve and the photospheric velocity evolution are both good and the solution is well constrained in the E-M_{He} plane. Lyman et al. (2014) found M_{ej}=1.7 M$_\odot$, E=1.2×10^{51} erg and M_{Ni}=0.22 M$_\odot$ using fits to the approximate Arnett (1982) models, which is consistent within error bars with our results.

SN 2006ba The bolometric lightcurve and photospheric velocity evolution of SN 2006ba is best fit with M_{He}=4.1 M$_\odot$, E=0.90×10^{51} erg and M_{Ni}=0.088 M$_\odot$. The fits to the bolometric lightcurve and the photospheric velocity evolution are both good (although there is only one photospheric velocity measurement) and the solution is well constrained in the E-M_{He} plane.

SN 2008aq The bolometric lightcurve and photospheric velocity evolution of SN 2008aq is best fit with M_{He}=3.3 M$_\odot$, and E=0.50×10^{51} erg and M_{Ni}=0.050 M$_\odot$. The fits to the bolometric lightcurve and the photospheric velocity evolution are both reasonably good and the solution is well constrained in the E-M_{He} plane.

SN 2009K The bolometric lightcurve and photospheric velocity evolution of SN 2009K is best fit with M_{He}=6.0 M$_\odot$, E=1.1×10^{51} erg and M_{Ni}=0.16 M$_\odot$. The fits to the bolometric lightcurve and the photospheric velocity evolution are both reasonably good. Due to the the missing lightcurve coverage after the peak, the constraint from the bolometric lightcurve is weak, and the solution is quite degenerate along the M/E=const curve.

SN 2009Z The bolometric lightcurve and photospheric velocity evolution of SN 2009Z is best fit with M_{He}=4.1 M$_\odot$, E=1.2×10^{51} erg and M_{Ni}=0.22 M$_\odot$. The fits to the bolometric lightcurve and the photospheric velocity evolution are both reasonably good. The solution is reasonably constrained in helium core mass but worse in explosion energy and is a bit degenerate along the M^2/E=const curve.

5.4. Results for the literature sample

Figure 12 shows the best-fit model bolometric lightcurve and photospheric velocity evolution compared to the (estimated) observed UV to MIR pseudo-bolometric lightcurve and estimated photospheric velocity evolution for the literature sample of Type IIb SNe. Table 2 gives the helium core mass, explosion energy, mass and mixing of ^{56}Ni, and explosion epoch for the best-fit models and the corresponding errors. Below we review the results and compare to other results obtained in the literature.

SN 1996cb The bolometric lightcurve and photospheric velocity evolution of SN 1996cb is best fit with M_{He}=4.9 M$_\odot$, E=1.4×10^{51} erg and M_{Ni}=0.11 M$_\odot$. The fits to the bolometric lightcurve and the photospheric velocity evolution are both good, but the solution is quite degenerate along the M/E=const curve suggesting that the constraint from the lightcurve is relatively
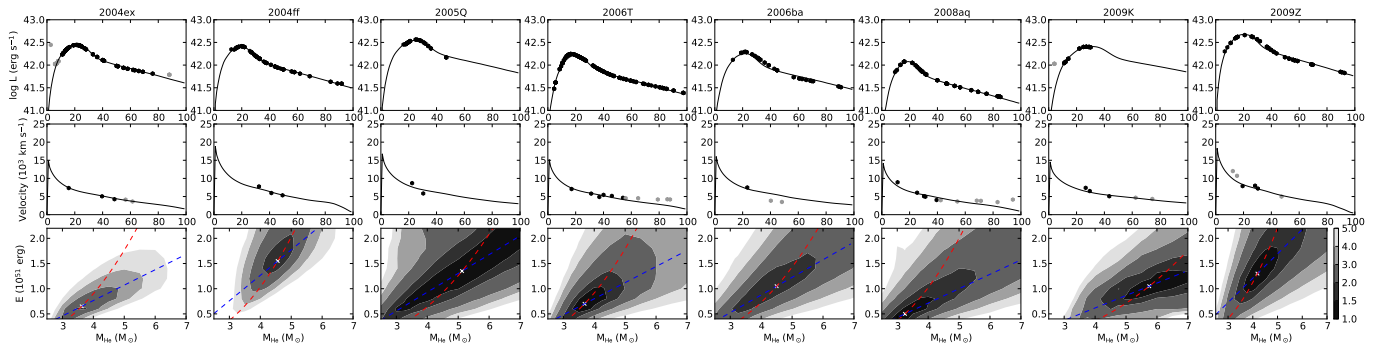
Fig. 11. Bolometric lightcurve (upper panels) and photospheric velocity evolution (lower panels) for the best-fit models as compared to the observed UV to MIR pseudo-bolometric lightcurve and estimated photospheric velocity evolution for the CSP sample of Type IIb SNe. The lower panels shows contour plots of the standard deviation in the fits, normalized to that of the optimal model, projected onto the E-M_{He} plane. We also show the constraints M_{ej}/E=const (blue) and M_{ej}^2/E=const (red) provided by the photospheric velocity evolution and the bolometric lightcurve, respectively.

Table 1. Helium core mass, explosion energy, mass of the ^{56}Ni and epoch of explosion for the best-fit models for the CSP sample of Type IIb SNe.

| SN | E | M_{He} | M_{Ni} | Mix_{Ni} | JD_{exp} |
	(10^{51} erg)	($M_\odot$)	($M_\odot$)		(days)
2004ex	0.65 (+0.40,-0.25)	3.62 (+0.56,-0.31)	0.131 (+0.044,-0.031)	1.23 (+0.25,-0.00)	53291.59 (+1.00,-1.41)
2004ff	1.60 (+0.63,-0.76)	4.56 (+0.44,-0.81)	0.113 (+0.019,-0.012)	1.20 (+0.28,-0.30)	53295.39 (+1.58,-1.58)
2005Q	1.10 (+0.81,-0.55)	4.50 (+1.23,-0.88)	0.181 (+0.038,-0.031)	1.20 (+0.28,-0.47)	53377.55 (+6.00,-2.50)
2006T	0.70 (+0.45,-0.30)	3.69 (+0.63,-0.50)	0.075 (+0.031,-0.019)	1.40 (+0.00,-0.30)	53770.71 (+1.25,-0.00)
2006ba	0.90 (+0.60,-0.38)	4.06 (+0.69,-0.73)	0.088 (+0.025,-0.019)	1.20 (+0.15,-0.40)	53808.31 (+1.50,-1.58)
2008aq	0.50 (+0.20,-0.10)	3.31 (+0.31,-0.06)	0.050 (+0.025,-0.018)	1.17 (+0.18,-0.27)	54517.44 (+1.80,-1.00)
2009K	1.10 (+0.75,-0.50)	6.00 (+1.12,-1.19)	0.163 (+0.044,-0.028)	1.17 (+0.05,-0.02)	54844.08 (+0.00,-0.00)
2009Z	1.25 (+0.90,-0.60)	4.06 (+0.81,-0.69)	0.225 (+0.031,-0.031)	1.40 (+0.00,-0.00)	54851.03 (+0.50,-0.00)
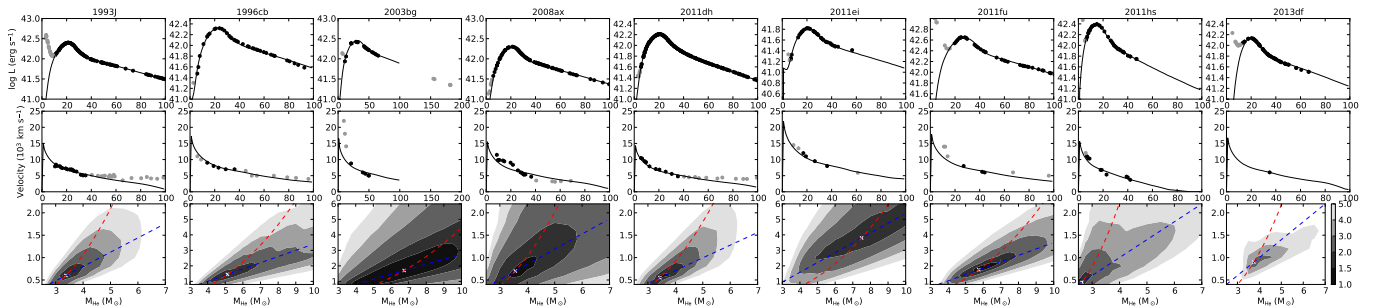
Fig. 12. Bolometric lightcurve (upper panels) and photospheric velocity evolution (lower panels) for the best-fit models as compared to the observed UV to MIR pseudo-bolometric lightcurve and estimated photospheric velocity evolution for the literature sample of Type IIb SNe. The lower panels shows contour plots of the standard deviation in the fits, normalized to that of the optimal model, projected onto the E-M_{He} plane. We also show the constraints M_{ej}/E=const (blue) and M_{ej}^2/E=const (red) provided by the photospheric velocity evolution and the bolometric lightcurve, respectively.

weak. Lyman et al. (2014) found M_{ej}=2.4 $M_\odot$, E=2.1×10^{51} erg and M_{Ni}=0.12 $M_\odot$ using fits to approximate Arnett (1982) models, which is consistent within error bars with our results.

SN 1993J The bolometric lightcurve and photospheric velocity evolution of SN 1993J is best fit with M_{He}=3.4 $M_\odot$, E=0.60×10^{51} erg and M_{Ni}=0.10 $M_\odot$. The fits to the bolometric lightcurve and the photospheric velocity evolution are good and the degeneracy of the solution is well constrained in the E-M_{He} plane. Shigeyama et al. (1994) found M_{He}=4.0 $M_\odot$, E=1.0-

1.2×10^{51} erg and M_{Ni}=0.073 $M_\odot$, and Woosley et al. (1994) found M_{He}=3.5 $M_\odot$, E=1.5×10^{51} erg and M_{He}=0.073 $M_\odot$ to well reproduce observations. These results are consistent within error bars with ours, except for the explosion energies which are considerably higher. The disagreement is likely caused by the presence of a relatively massive hydrogen envelope (Sect. 4), as suggested by the extent of the cooling phase. The explosion energy deposited in the helium core for the Shigeyama et al. (1994) models was ~0.6×10^{51} erg, which is in agreement with our result.

Table 2. Helium core mass, explosion energy, mass of the ^{56}Ni and epoch of explosion for the best-fit models for the literature sample of Type IIb SNe.

SN	E $(10^{51}$ erg)	M_{He} $(M_{\odot})$	M_{Ni} $(M_{\odot})$	Mix_{Ni}	JD_{exp} (days)
1996cb	1.40 (+0.89,-0.65)	4.88 (+1.01,-0.96)	0.106 (+0.170,-0.067)	0.95 (+0.30,-0.10)	50428.50 (+1.22,-5.50)
1993J	0.60 (+0.45,-0.20)	3.38 (+0.60,-0.34)	0.100 (+0.042,-0.020)	0.90 (+0.20,-0.08)	49074.00 (+0.00,-0.00)
2003bg	1.55 (+1.26,-0.68)	6.38 (+1.79,-1.29)	0.175 (+0.108,-0.071)	1.00 (+0.00,-0.00)	52701.50 (+0.00,-3.00)
2008ax	0.65 (+0.60,-0.25)	3.44 (+0.84,-0.40)	0.081 (+0.042,-0.041)	0.93 (+0.04,-0.04)	54528.80 (+0.00,-0.00)
2011dh	0.55 (+0.40,-0.15)	3.44 (+0.65,-0.25)	0.075 (+0.028,-0.020)	1.10 (+0.11,-0.00)	55713.00 (+0.00,-0.00)
2011ei	3.80 (+2.20,-1.59)	7.38 (+0.76,-1.30)	0.032 (+0.011,-0.011)	1.00 (+0.00,-0.00)	55772.00 (+1.00,-1.66)
2011fu	1.75 (+1.31,-0.81)	5.75 (+1.43,-1.12)	0.231 (+0.093,-0.101)	1.00 (+0.00,-0.00)	55823.50 (+3.16,-1.12)
2011hs	0.45 (+0.26,-0.05)	2.62 (+0.25,-0.06)	0.088 (+0.059,-0.036)	1.40 (+0.00,-0.40)	55869.00 (+1.87,-0.87)
2013df	0.95 (+0.60,-0.46)	3.81 (+0.50,-0.75)	0.056 (+0.000,-0.009)	0.70 (+0.00,-0.07)	56446.80 (+0.00,-1.73)

SN 2003bg The bolometric lightcurve and photospheric velocity evolution of SN 2003bg is best fit with M_{He}=6.4 $M_{\odot}$, E=1.6×10^{51} erg and M_{Ni}=0.18 $M_{\odot}$. The fits to the bolometric lightcurve and the photospheric velocity evolution are acceptable, but the solution is quite degenerate along the M/E=const curve. This suggests that the constraint from the lightcurve is relatively weak, which is not surprising given the sparse sampling during the diffusion peak. Mazzali et al. (2009) find M_{ej}=3.9-4.8 $M_{\odot}$, E=5×10^{51} erg and M_{Ni}=0.15-0.18 $M_{\odot}$ to well reproduce observations. This is consistent within error bars with our results, except for the explosion energy which is considerably higher. The disagreement could be caused by the presence of a relatively massive hydrogen envelope (Sect. 4), although there is only a hint of a cooling phase in the earliest observations. According to Mazzali et al. (2009) the kinetic energy of the helium core was ≲2.5×10^{51}, which is in better agreement with our result.

SN 2008ax The bolometric lightcurve and photospheric velocity evolution of SN 2008ax is best fit with M_{He}=3.4 $M_{\odot}$, E=0.65×10^{51} erg and M_{Ni}=0.081 $M_{\odot}$. The fit to the bolometric lightcurve is good whereas the fit to the photospheric velocity evolution is a bit worse, and the solution is reasonable well constrained in the E-M_{He} plane. Tsvetkov et al. (2009) find M_{He}=3.5 $M_{\odot}$, E=1.5×10^{51} erg and M_{Ni}=0.11 $M_{\odot}$ to well reproduce observations using the SN 1993J model 13C from Woosley et al. (1994), with M_{Ni} adjusted to match SN 2008ax. These results are consistent within error bars with ours, except the explosion energy which is condsiderably higher. However, in this case the situation is reversed as compared to SN 1993J. The absence of an extended cooling phase suggests a relatively low-mass hydrogen envelope for SN 2008ax, so the SN 1993J based model used by Tsvetkov et al. (2009) could lead to a significant overestimate of the explosion energy (Sect. 4).

SN 2011dh The bolometric lightcurve and photospheric velocity evolution of SN 2011dh is best fits with a helium core mass of 3.44 $M_{\odot}$, and explosion energy of 0.55×10^{51} erg and a mass of ^{56}Ni of 0.075 $M_{\odot}$. The fits to the bolometric lightcurve and the photospheric velocity evolution are good and the solution is well constrained in the E-M_{He} plane. Bersten et al. (2012) found M⊙3.3-4.0 $M_{\odot}$, E=0.6-1.0×10^{51} erg and M_{Ni}=0.05-0.010 $M_{\odot}$ (adjusted in Ergon et al. 2014b) to well reproduce obser-

vations. These results are consistent within error bars with our results, which are also in good agreement with those obtained in Ergon et al. (2014a) based on the <400 days lightcurve and an extended version of the model grid using a bolometric correction determined with steady-state NLTE modelling.

SN 2011ei The bolometric lightcurve and photospheric velocity evolution of SN 2011ei is best fit with M_{He}=7.4 $M_{\odot}$, E=3.8×10^{51} erg and M_{Ni}=0.032 $M_{\odot}$. The fits to the bolometric lightcurve and the photospheric velocity evolution are both good, but due to the limited tail coverage the constraint from the bolometric lightcurve is relatively weak, and the solution quite degenerate along the M/E=const curve. This SN shows the most extreme values for the SN and progenitor parameters in the sample. Whereas the helium core mass and explosion energy are the highest, the mass of ^{56}Ni is the lowest. The high helium core mass and explosion energy derived stem mainly from the unusually high photospheric velocities, whereas the time at which peak luminosity occurs is quite typical. The small ejecta mass of 0.3 $M_{\odot}$ estimated from modelling of nebular spectra in Milisavljevic et al. (2013) seems to be excluded by our results.

SN 2011fu The bolometric lightcurve and photospheric velocity evolution of SN 2011fu is best fit with M_{He}=5.8 $M_{\odot}$, E=1.8×10^{51} erg and M_{Ni}=0.23 $M_{\odot}$. The fits to the bolometric lightcurve and the photospheric velocity evolution are reasonably good and the degeneracy of the solution acceptable, although there is clear degeneracy along the M/E=const curve suggesting that the constraint from the lightcurve is relatively weak.

SN 2011hs The bolometric lightcurve and photospheric velocity evolution of SN 2011hs is best fit with M_{He}=2.6 $M_{\odot}$, E=0.45×10^{51} erg and M_{Ni}=0.088 $M_{\odot}$. The fits to the bolometric lightcurve and the photospheric velocity evolution are good and the degeneracy of the solution is well constrained above in the E-M_{He} plane. However, the solution lies at the border of the covered parameter space and is not well constrained below. Bufano et al. (2014) found M_{He}=3.3-4 $M_{\odot}$, E=0.6-0.9×10^{51} erg and M_{Ni}=0.037-0.040 $M_{\odot}$ of ^{56}Ni to well reproduce the observations. The lower bound on the explosion energy is consistent within error bars with our result, whereas the lower bound on helium core mass and the upper bound on the mass of ^{56}Ni lies just
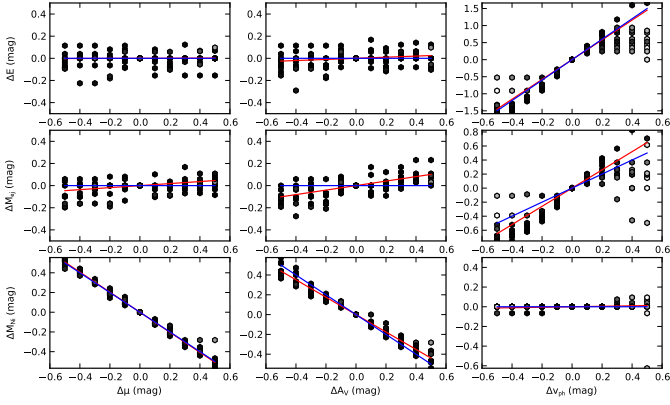
Fig. 13. Sensitivity of the derived explosion energy (upper panels), ejecta mass (middle panels), mass of ^{56}Ni (lower panels) to a change in the distance (left panels), extinction (middle panels) and photospheric velocities (right panels). For consistency the changes in all quantities are expressed in magnitudes. The derived quantities for the CSP and literature samples of Type IIb SNe are shown as black dots, power-law fits as red solid lines and the scalings expected from the Arnett (1982) model as blue solid lines.

outside our error bars. It is worth noting that the lower bounds on the explosion energy and helium core mass, which agrees best with our results, corresponds to the case of strong mixing of the ^{56}Ni, in agreement with our results. The results in Bufano et al. (2014) were obtained with the hydrodynamical code presented by Bersten et al. (2011) which, as previously discussed, is very similar to HYDE.

SN 2013df The bolometric lightcurve and photospheric velocity evolution of SN 2011df is best fit with M_{He}=3.8 $M_\odot$, E=0.95×10^{51} erg and M_{Ni}=0.056 $M_\odot$. The fits to the bolometric lightcurve and the photospheric velocity evolution are good and the degeneracy of the solution is well constrained in the E-M_{He} plane. Morales-Garoffolo et al. (2014) found M_{ej}=0.8-1.4, E=0.4-1.2×10^{51} erg and M_{Ni}=0.1 $M_\odot$ using fits to approximate Arnett (1982) models. The explosion energy is consistent within error bars with our results, whereas the ejecta mass is below and the mass of ^{56}Ni above our error bars, the latter partly explained by the difference in the adopted distance.

5.5. Error sensitivity

Fig. 13 shows the sensitivity of the derived quantities to errors in the distance, extinction and a systematic error in the photospheric velocity for the CSP and literature samples of Type IIb SNe. To compare with approximate scalings we have replaced the helium core mass with the ejecta mass. For the ejecta mass and explosion energy the dependence on the distance and extinction is weak, whereas the dependence on the photospheric velocity is strong. For the mass of ^{56}Ni the sensitivity on the distance and extinction is strong whereas the dependence on the photospheric velocity is weak. In general we see that an error in the distance and extinction mainly corresponds to an error in the mass of ^{56}Ni, whereas an error in the photospheric velocity mainly corresponds to an error in the helium core mass and explosion energy. This behaviour is in agreement with the model grid dependencies discussed in Sect. 3.3 and with the qualitative discussion in E14a, based on the Arnett (1982) model. In Fig. 13 we show the scalings expected from the Arnett (1982)
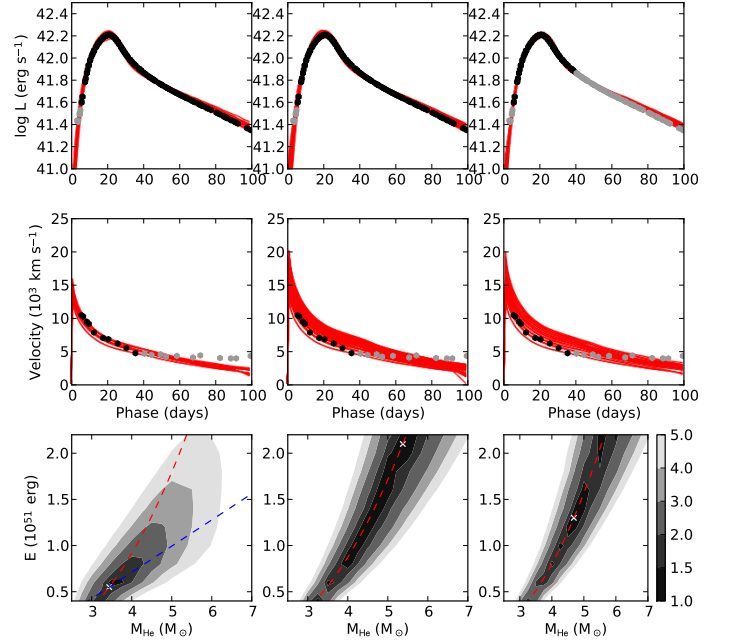
Fig. 14. Model bolometric lightcurve (upper panels) and photospheric velocity evolution (middle panels) as compared to the observed UV to MIR pseudo-bolometric lightcurve and estimated photospheric velocity evolution for SN 2011dh. Models with a normalized standard deviation <2 are shown in red for the cases when the lightcurve and photospheric velocity evolution (left panels), only the lightcurve (middle panels) and only the diffusion phase lightcurve (right panels) where used in the fit. The lower panels shows the corresponding contour plots displayed as in Figs. 11 and 12.

model and, as previously found in Sect. 3.3, these are well followed by the model grid.

5.6. Degeneracy of the solution

Fig. 14 shows the bolometric lightcurve and photospheric velocity evolution for models with a normalized standard deviation <2 as compared to observations for SN 2011dh. The left, middle and right panels show the cases when lightcurve and photospheric velocity evolution, only the lightcurve and only the diffusion phase lightcurve were used in the fit, respectively. The lower panels shows the corresponding contour plots and in the two latter cases, where the photospheric velocity evolution is not used in the fit, the solution is completely degenerate. This is not obvious as the diffusion phase and tail phase lightcurves might provide independent constraints arising from the diffusion time for thermal radiation and the optical depth for γ-rays, respectively. In E14a we argued that this could be the case, given that the diffusion time and optical depth provide the constraints M_{ej}^3/E=const and M_{ej}^2/E=const, respectively, in the Arnett (1982) model. However, as discussed in Sect. 3.3, this model assumes a constant opacity and the constraint provided by diffusion phase lightcurve is rather M_{ej}^2/E=const for the hydrodynamical models. Therefore the diffusion phase and tail phase lightcurves appears to provide similar constraints and, as seen in the middle and right panels of Fig. 14, the degeneracy regions well follows the M_{ej}^2/E=const relation. The photospheric velocity evolution is expected to provide a constraint similar to M_{ej}/E=const, which would break the degeneracy and, as seen in the left panels of
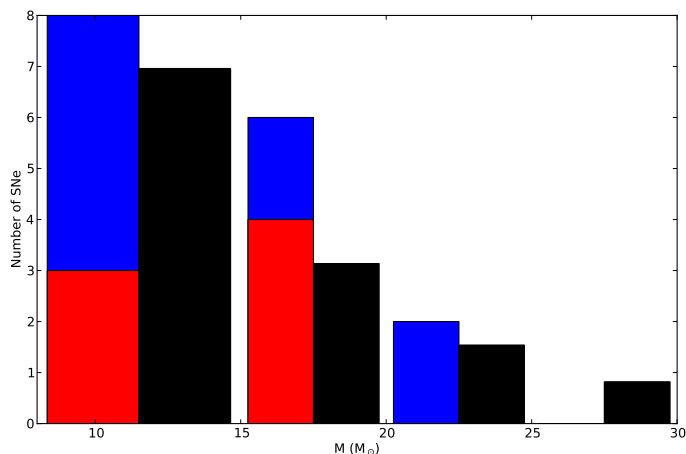
Fig. 16. Number of SNe with initial mass in the 8-15, 15-20, 20-25 and 25-30 $M_\odot$ bins for the CSP (blue) and literature (red) samples of Type IIb SNe as compared to a standard Salpeter IMF (black).

Fig. 14, this is also the case. We have exemplified with SN 2011dh but the conclusion is the same for the other SNe in the CSP and literature samples.

5.7. Sample statistics

No parameter studies specifically aimed at Type IIb SNe have been published, but the stripped-envelope SN parameter study by Lyman et al. (2014) include all Type IIb SNe from the literature sample except SNe 2011fu, 2011ei and 2013df. On the other hand, their sample includes the Type IIb SN 2004el missing from ours. Their results are based on the approximate (Arnett 1982) model, but are nevertheless interesting to compare with. Fig. 15 shows E versus M_{He} (left panel), M_{Ni} versus M_{He} (middle panel) and M_{Ni} versus E (right panel) for the combined CSP and literature sample of Type IIb SNe. The caveat that the explosion energy might be underestimated for some SNe with more massive hydrogen envelopes (Sect. 4.1) should be kept in mind.

We find a correlation between E and M_{He}, best fitted with a power law with index 1.8. Some caution is advised as this is similar to the M_{ej}^2/E=const degeneracy curve (Sect. 5.6). However, the SNe that obviously belongs to the low and high mass ends, like SN 2011hs and 2003bg, well follows the relation. Lyman et al. (2014) also find a correlation, and assuming a mass for the compact remnant of 1.5 $M_\odot$, their results for the Type IIb SNe are best fitted with a power law with index of 1.8, in agreement with our results. The correlation found is also in qualitative agreement with the relation between progenitor mass and explosion energy for Type IIP SNe suggested by Poznanski (2013), which has a power law index of 3.

We find correlations between M_{Ni} and E and between M_{Ni} and M_{He}, best fitted with power laws with indices 0.7 and 1.1, respectively. Lyman et al. (2014) also find correlations between these quantities, and assuming a mass for the compact remnant of 1.5 $M_\odot$, their results for the Type IIb SNe are best fitted with power laws with indices of 0.89 and 1.36, respectively, in good agreement with our results. Hamuy (2003) find a correlation between M_{Ni} and E for Type IIP SNe, using relations derived from model grid fits by Litvinova & Nadezhin (1983, 1985), and their results are best fitted with a power law with index 0.88, in good agreement with our results for Type IIb SNe. The correlations found are also in qualitative agreement with the relations between progenitor mass and M_{Ni} and expansion velocities and

M_{Ni} for Type IIP SNe found by Fraser et al. (2011) and Maguire et al. (2012), respectively. We note that SN 2011ei is an extreme outlier in the M_{Ni} versus M_{He} and M_{Ni} versus E figures, suggesting a different nature of this SN as compared to the other.

Fig.16 shows the number of SNe with initial mass in the 8-15, 15-20, 20-25 and 25-30 $M_\odot$ bins for the combined CSP and literature sample of Type IIb SNe as compared to a standard Salpeter IMF. We find 6 SNe instead of the expected 3 SNe in the 15-20 $M_\odot$ bin and no SNe instead of the expected 4 SNe in the >25 $M_\odot$ bins. Except for this there are no significant deviations from a standard Salpeter IMF. We find 50 percent of the SNe in the <15 $M_\odot$ bin and 88 percent of the SNe in the <20 $M_\odot$ bins. The results for the Type IIb SNe from Lyman et al. (2014) are similar, with 67 percent of the SNe in the <15 $M_\odot$ bin and 100 percent of the SNe in the <20 $M_\odot$ bins. Given the current estimates of stellar mass loss rates (references) the implication of our result is quite clear; either the binary channel is dominating the production of Type IIb SNe or these rates needs a serious revision. The idea that Type IIb SNe arise mainly from the binary channel has been proposed by several authors (references), but the size of the sample and the relatively detailed modelling used strengthens the support for this scenario considerably.

6. Conclusions

We present HYDE, a new one-dimensional hydrodynamical code and use it to build a grid of SN models based on bare helium core models evolved with MESA STAR. Such a grid is well suited to model the diffusion and early tail phase of Type IIb SNe, as the progenitors of these are thought to have lost all but a tiny fraction of their hydrogen envelopes. We investigate the dependence of the observed quantities on the progenitor and SN parameters, and find these to qualitatively follow expectations from the approximate Arnett (1982) model. However, significant quantitative differences do exist, likely because of the constant opacity assumed in this model. We also investigate the effects of a low-mass hydrogen envelope on the observed properties, and find these to be negligible after the luminosity minimum, expect for relatively massive hydrogen envelopes, where the photospheric velocities are decreased, likely because of deceleration of the helium core.

We use an automated fitting procedure to fit the bolometric lightcurves and photospheric velocities for the CSP and literature samples of Type IIb SNe to this grid of SN models. This allows us to take into account the uncertainties in distance, extinction and photospheric velocities, as well as to investigate the degeneracy of the solutions. We find SN and progenitor parameters in reasonable agreement with previous hydrodynamical modelling for SNe 1993J, 2003bg, 2008ax, 2011dh, 2011hs and 2003bg. However, in the case of 1993J and 2003bg, the derived explosion energies are significantly lower, likely due to the effect of their relatively massive hydrogen envelopes. For SN 2011ei we find an initial mass quite different from that obtained by modelling of nebular spectra in Milisavljevic et al. (2013). We find an almost complete degeneracy in the helium core mass and explosion energy along the M_{ej}^2/E=const curve if the photospheric velocities are not used in the fit. When these are included the degeneracy is broken and the fit becomes quite robust. We find an error in the distance and extinction to propagate mainly to derived the mass of ^{56}Ni, and a systematic error in the photospheric velocity to propagate mainly to the derived helium core mass and explosion energy.

We find correlations between the SN and progenitor parameters, the explosion energy increasing with helium core mass,
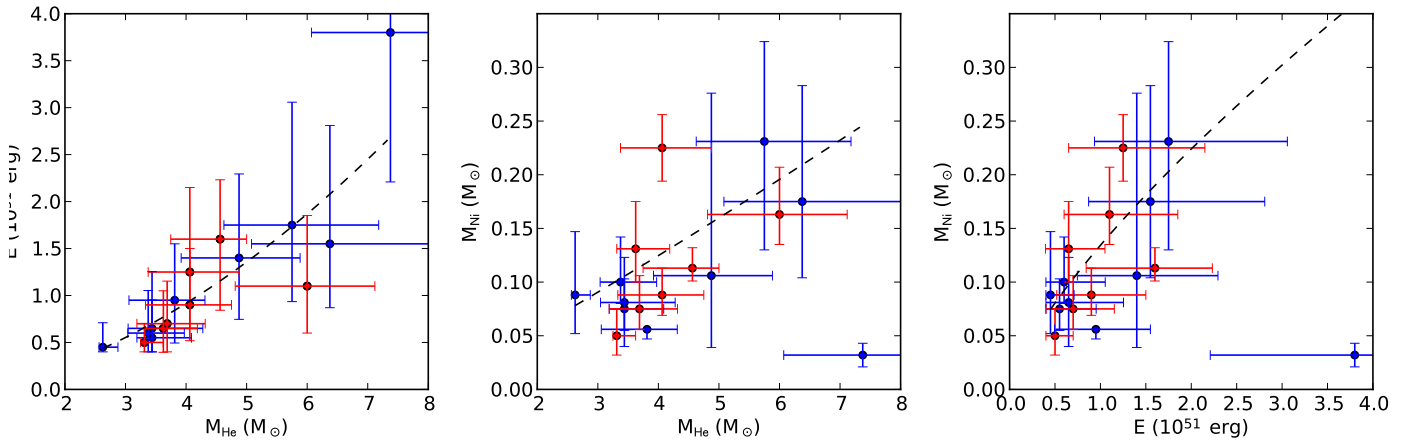
Fig. 15. E versus M_{He} (left panel), M_{Ni} versus M_{He} (middle panel) and M_{Ni} versus E (right panel) for the CSP (blue) and literature (red) samples of Type IIb SNe. We also show power law fits as black dashed lines.

and the mass of ^{56}Ni increasing with the explosion energy. The former correlation is best fitted with power-law index of 1.8 and the latter with a power-law index of 1.1, in good agreement with the results in Lyman et al. (2014), obtained for a smaller sample using the approximate Arnett (1982) model. The initial masses of the combined CSP and literature samples follows a standard Salpeter IMF reasonably well, although there is an overpopulation in the 15-20 $M_\odot$ bin and an underpopulation in the >25 $M_\odot$ bins. The fraction of SNe with mass <15 $M_\odot$ and <20 $M_\odot$ are 50 and 88 percent, respectively, in good agreement with the results in Lyman et al. (2014). The implication of this result is quite clear; either the binary channel is dominating the production of Type IIb SNe or stellar massloss rates are considerably higher than expected. This conclusion is not new, and the evidence for this have been growing since the discovery of SN 1993J, but the size of the sample and the relatively detailed modelling used strengthen it considerably.

7. Acknowledgements

Appendix A: The CSP sample of Type IIb SNe

The Type IIb SNe in the CSP sample consists of SNe 2004ex, 2004ff, 2005Q, 2006T, 2006ba, 2006bf, 2008aq, 2009K, 2009Z and 2009dq. The observational data for these SNe are described in Taddia et al. (2014) and SNe 2006bf and 2009dq have been excluded due to bad sampling of the lightcurves. The photospheric velocities were estimated from the absorption minimum of the Fe II 5169 Å line, in turn measured from the observed spectra as described in Taddia et al. (2014). Wherever used, the line-of-site extinction within the Milky way have been adopted from the Schlegel et al. (1998) extinction maps, recalibrated by Schlafly & Finkbeiner (2011).

SN 2004ex   Discovered 2004 Oct 11.34 UT (Jacques et al. 2004) in NGC 182 at an apparent magnitude of 17.7, and the explosion epoch is constrained by non-detections from Oct 6.35 UT (<20.0 mag) and 10.33 (<19.0 mag) (Shimasaki et al. 2004). The photometric data covers the u to H bands and the 5-85 days period after discovery. Both the diffusion peak and early tail are well covered. The distance modulus for the NGC 182 was adopted as the median and standard deviation of the literature values given by the NASA/IPAC Extragalactic Database

(NED), being 34.83±0.27 mag. The line-of-sight extinction within NGC 182 was estimated to $E(B-V)_H$=0.078 mag by comparison of the V-i colour at r-band maximum with SN 2011dh. Adding the line-of-sight-extinction within the Milky Way ($E(B-V)_{MW}$=0.021 mag) gives $E(B-V)$=0.099 mag. The pseudo-bolometric UV to MIR bolometric lightcurve was calculated using the $uBVriJH$ bands.

SN 2004ff   Discovered 2004 Oct 30.40 UT (Pugh et al. 2004) in ESO 552-G40 at an apparent magnitude of 18.0, and the explosion epoch is constrained by a non-detections from 2004 Oct 13.41 (<19.0 mag) and 21.40 UT (<18.0 mag) (Pugh et al. 2004). The photometric data covers the u to H band and the 5-80 days period after discovery. The rise to peak is not well covered and we have included observations from Pugh et al. (2004) to extend this coverage. In the absence of literature measurements of the distance to ESO 552-G40 we adopt the Virgo, Great Attractor and Shapley corrected kinematic distance modulus given by NED, being 34.82±0.15 mag. The line-of-sight extinction within ESO 552-G40 was estimated to $E(B-V)_H$=0.138 mag by comparison of the V-i colour at r-band maximum with SN 2011dh. Adding the line-of-sight-extinction within the Milky Way ($E(B-V)_{MW}$=0.029 mag) gives $E(B-V)$=0.167 mag. The pseudo-bolometric UV to MIR bolometric lightcurve was calculated using the $uBVriJH$ bands.

SN 2005Q   Discovered 2005 Jan 28.80 UT (Monard 2005) in ESO 244-G31 at an apparent magnitude of 17.2, and the explosion epoch is constrained by a non-detection from 2004 Dec 30.81 UT (<18.7 mag). The photometric data covers the u to i bands and the 0-50 days period after discovery. The rise to peak and the early tail is not well covered. The distance modulus for ESO 244-G31 was adopted as the median and standard deviation of the literature values given by NED, being 34.83±0.18 mag. The V-i colour at r-band maximum was bluer than for SN 2011dh, so the line-of-sight extinction within ESO 244-G31 was assumed to be negligible. The line-of-sight-extinction within the Milky Way is $E(B-V)_{MW}$=0.023 mag. The pseudo-bolometric UV to MIR bolometric lightcurve was calculated using the $uBVri$ bands.

SN 2006T   Discovered 2006 Jan 30.99 UT (Monard 2006b) in NGC 3054 at an apparent magnitude of 17.2, and the explosion epoch is constrained by a non-detection from 2006 Jan 16.96 UT (<18.0 mag) (Monard 2006b). The photometric data covers the u to H bands and the 0-125 days period after discovery. Both the diffusion peak and the early tail are well covered. The distance modulus for NGC 3054 was adopted as the median and standard deviation of the literature values given by NED, being 32.58±0.35 mag. The V-i colour at r-band maximum was bluer than for SN 2011dh, so the line-of-sight extinction within NGC 3054 was assumed to be negligible. The line-of-sight-extinction within the Milky Way is $E(B\text{-}V)_{\rm MW}$=0.181 mag. The pseudo-bolometric UV to MIR bolometric lightcurve was calculated using the $uBVriJH$ bands.

SN 2006ba   Discovered 2006 Mar 19.81 UT (Monard 2006a) in NGC 2980 at an apparent magnitude of 17.7, and the explosion epoch is constrained by a non-detection from 2006 Feb 5.04 UT (<18.8) (Monard 2006a). The photometric data covers the u to H bands and the 5-80 days period after discovery. The rise to peak is not well covered. The distance modulus for NGC 2980 was adopted as the median and standard deviation of the literature values given by NED, being 34.48±0.26 mag. The line-of-sight extinction within NGC 2980 was estimated to $E(B\text{-}V)_{\rm H}$=0.212 by comparison of the V-i colour at r-band maximum with SN 2011dh. Adding the line-of-sight-extinction within the Milky Way ($E(B\text{-}V)_{\rm MW}$=0.046) gives $E(B\text{-}V)$=0.258. The pseudo-bolometric UV to MIR bolometric lightcurve was calculated using the $BVriJ$ bands.

SN 2008aq   Discovered 2008 Feb 27.44 UT (Chu et al. 2008) in MCG -02-33-20 at an apparent magnitude of 16.3, and the explosion epoch is constrained by a non-detection from 2008 Feb 10.47 UT (<19.1 mag) (Chu et al. 2008). The photometric data covers the u to H bands and the 5-120 days period after discovery. The rise to peak is not well covered but we have included observations from Chu et al. (2008) and Brown et al. (2008) to extend this coverage. The distance modulus for MCG -02-33-20 was adopted as the median and standard deviation of the literature values given by NED, being 32.45±0.43, 0.43 mag. The V-i colour at r-band maximum was bluer than for SN 2011dh so the line-of-sight extinction within MCG -02-33-20 was assumed to be negligible. The line-of-sight-extinction within the Milky Way is $E(B\text{-}V)_{\rm MW}$=0.040 mag. The pseudo-bolometric UV to MIR bolometric lightcurve was calculated using the $uBVriJH$ bands.

SN 2009K   Discovered 2009 Jan 14.07 UT (Pignata et al. 2009) in NGC 1620 at an apparent magnitude of 14.9, and the explosion epoch is constrained by a non-detection from 2009 Jan 11.08 UT (<18.0 mag) (Pignata et al. 2009). The photometric data covers the B to H bands and the 0-50 days period after discovery. The early tail is not covered. The distance modulus for NGC 1620 was adopted as the median and standard deviation of the literature values given by NED, being 33.15±0.22 mag. The line-of-sight extinction within NGC 1620 was estimated to $E(B\text{-}V)_{\rm H}$=0.057 mag by comparison of the V-i colour at r-band maximum with SN 2011dh. Adding the line-of-sight-extinction within the Milky Way ($E(B\text{-}V)_{\rm MW}$=0.051 mag) gives $E(B\text{-}V)$=0.108 mag. The pseudo-bolometric UV to MIR bolometric lightcurve was calculated using the $uBVri$ bands.

SN 2009Z   Discovered 2009 Feb 2.53 UT (Griffith et al. 2009) in SDSS J140153.80-012035.5 at an apparent magnitude of 18.1, and the explosion epoch is constrained by a non-detection from 2008 Jun-Jul (<19.4 mag) (Griffith et al. 2009). The photometric data covers u to i bands and the 5-85 days period after discovery, although additional NIR photometry where obtained at ~400 days. The rise to peak is not well covered but we have included observations from Griffith et al. (2009) to extend this coverage. In the absence of literature measurements of the distance to SDSS J140153.80-012035.5 we adopt the the Virgo, Great Attractor and Shapley corrected kinematic distance modulus given by NED, being 35.26±0.15 mag. The V-i colour at r-band maximum was bluer than for SN 2011dh so the line-of-sight extinction within SDSS J140153.80-012035.5 was assumed to be negligible. The line-of-sight-extinction within the Milky Way is $E(B\text{-}V)_{\rm MW}$=0.042 mag. The pseudo-bolometric UV to MIR bolometric lightcurve was calculated using the $uBVri$ bands.

Appendix B: The literature sample of Type IIb SNe

The Type IIb SNe in the literature sample consists of SNe 1993J (e.g. Richmond et al. 1994, 1996), 1996cb (Qiu et al. 1999), 2003bg (Hamuy et al. 2009), 2008ax (e.g. Taubenberger et al. 2011), 2011dh (e.g. Ergon et al. 2014b), 2011fu (Kumar et al. 2013), 2011hs (Bufano et al. 2014), 2011ei (Milisavljevic et al. 2013) and 2013df (Van Dyk et al. 2014). Wherever used, the line-of-site extinction within the Milky way have been adopted from the Schlegel et al. (1998) extinction maps, recalibrated by Schlafly & Finkbeiner (2011).

SN 1996cb   Discovered 1996 Dec 15.71 UT (Nakano et al. 1996) in NGC 3510 at an apparent magnitude of 16.5, and the explosion epoch is constrained by a non-detection from 1996 Nov 29 UT (<19.0 mag) (Qiao et al. 1996). The photometric data was taken from Qiu et al. (1999) and covers the B to R bands and the 5-160 days period after discovery. To extend the rise to peak coverage we also included observations from (Nakano et al. 1996) and (Qiao et al. 1996). The distance modulus for NGC 3510 was adopted as the mean and standard deviation of the literature values given by NED being 30.57±1.03. The total line-of-sight extinction was taken as the mean of the upper limit determined by Qiu et al. (1999) from comparison to SN 1993J ($E(B\text{-}V)$=0.12) and the line-of-sight extinction within the Milky Way ($E(B\text{-}V)$=0.12), giving $E(B\text{-}V)$=0.073±0.047. The pseudo-bolometric UV to MIR bolometric lightcurve was calculated using the BVR bands. Estimates of the photospheric velocities using SYNOW were adopted from Deng et al. (2001). This method has been shown by Takáts & Vinkó (2012) to give results similar to those obtained from the absorption minimum of Fe ɪɪ 5169 Å line for a sample of Type IIP SNe.

SN 2003bg   Discovered 2003 Feb 25.70 UT (Wood-Vasey et al. 2003) in MCG -05-10-15 at an apparent magnitude of 15.0, and the explosion epoch is constrained by a non-detection from 2002 Nov 7.0 UT (<18.0 mag) (Wood-Vasey et al. 2003). The photometric data was taken from Hamuy et al. (2009) and covers the B to K bands and the 5-325 days period after discovery. The distance modulus for the host galaxy MCG-05-10-015 was adopted from Kelson et al. (2000), and the total line-of-sight extinction taken as the mean of the line-of-sight extinction within the Milky Way ($E(B\text{-}V)$=0.02) and an assumed upper limit of 0.1 mag additional extinction, giving $E(B\text{-}V)$=0.070±0.05. The

pseudo-bolometric UV to MIR bolometric lightcurve was calculated using the *BVRIJHK* bands. Estimates of the photospheric velocities using the Monte Carlo (MC) radiative transfer code by Mazzali & Lucy (1993); Lucy (1999); Mazzali (2000) was adopted from Mazzali et al. (2009).

SN 2011ei Discovered 2011 Jul 25.43 UT (Marples et al. 2011) in NGC 6925 at an apparent magnitude of 18.0, and the explosion epoch is constrained by a non-detection from 2011 Jun 23.58 UT (<19.1 mag) (Marples et al. 2011). The photometric data was taken from Milisavljevic et al. (2013) and covers *U* to *I* bands and the 0-50 days period. The distance modulus for the host galaxy NGC 6925 was adopted as the mean and standard deviation of the literature values given by NED being 32.42±0.27. The total line-of-sight extinction was taken as the mean of the upper limit determined by Milisavljevic et al. (2013) ($E(B-V)$=0.232), who used the equivalent width of the interstellar Na ı D interstellar absorption lines and the relation between this and $E(B-V)$ by Turatto et al. (2003), and the line-of-sight-extinction within the Milky Way ($E(B-V)$=0.052), giving $E(B-V)$=0.142±0.09. The pseudo-bolometric UV to MIR bolometric lightcurve was calculated using the *UBVRI* bands. Estimates of the photospheric velocities using SYNOW was taken from Milisavljevic et al. (2013).

SN 2011fu Discovered 2011 Sep 21.04 UT (Ciabattari et al. 2011) in UGC 1626 at an apparent magnitude of 15.8, and the explosion epoch is constrained by a non-detection from 2011 Aug 10 UT (<18.8 mag) (Ciabattari et al. 2011). The photometric data covers the *U* to *I* bands and the 10-175 days period and was taken from Kumar et al. (2013). In the absence of literature measurements of the distance to the host galaxy UGC 1626 we adopt the Virgo, Great Attractor and Shapley corrected kinematic distance modulus given by NED, being 34.36 and assume an error in this estimate of 50 percent. The total line-of-sight extinction was adopted from Kumar et al. (2013), who used the equivalent width of the interstellar Na ı D interstellar absorption lines and the relation between this and $E(B-V)$ by Munari & Zwitter (1997) to estimate $E(B-V)$=0.22±0.11. The pseudo-bolometric UV to MIR bolometric lightcurve was calculated using the *UBVRI* bands. Measurements of the absorption minimum of Fe ıı 5169 Å line was taken from Kumar et al. (2013).

SN 2011hs Discovered 2011 Nov 12.48 UT (Drescher et al. 2011) in IC 5267 at an apparent magnitude of 15.5, and the explosion epoch is constrained by a non-detection from 2011 Oct 9.574 UT (<18.7 mag) (Drescher et al. 2011). The photometric data covers the *U* to *K* bands and 0-120 days period and was taken from Bufano et al. (2014). The distance modulus for the host galaxy IC 5267 was adopted as the mean and standard deviation of the literature values given by NED, being 32.05±0.41. The total line-of-sight extinction was adopted from Bufano et al. (2014), who used the equivalent width of the interstellar Na ı D interstellar absorption lines and the relation between this and $E(B-V)$ by Poznanski et al. (2012) to estimate $E(B-V)$=0.17±0.08. The pseudo-bolometric UV to MIR bolometric lightcurve was calculated using the *UBVRIJH* bands. Spectroscopic data was taken from Bufano et al. (2014), and the photospheric velocities estimated from the absorption minimum of the Fe ıı 5169 Å line, in turn measured with a simple automated algorith described in E14a.

SN 2013df Discovered 2013 Jun 7.87 UT (Ciabattari et al. 2013) in NGC 4414 at an apparent magnitude of ?.?, and the explosion epoch is constrained by a non-detection from 2013 ? ?.? UT (<?.= mag) (Ciabattari et al. 2013). The photometric data covers the *B* to *H* bands and the 5-65 days period and was taken from Van Dyk et al. (2014). The distance modulus for the host galaxy NGC 4414 was taken as the Cepheid based measurement by Freedman et al. (2001), being 31.10±0.05. The total line-of-sight extinction was adopted from Van Dyk et al. (2014), which used the equivalent width of the interstellar Na ı D interstellar absorption lines and the relation between this and $E(B-V)$ by Poznanski et al. (2012) to estimate $E(B-V)$=0.097±0.016. The pseudo-bolometric UV to MIR bolometric lightcurve was calculated using the *BVRIzJH* bands. The spectroscopic data was taken from Van Dyk et al. (2014) and the photospheric velocities estimated from the absorption minimum of the Fe ıı 5169 Å line in turn measured with a simple automated algorithm described in E14a.

References

Alexander, D. R. & Ferguson, J. W. 1994, ApJ, 437, 879
Arnett, W. D. 1982, ApJ, 253, 785
Bersten, M. C., Benvenuto, O., & Hamuy, M. 2011, ApJ, 729, 61
Bersten, M. C., Benvenuto, O. G., Nomoto, K., et al. 2012, ApJ, 757, 31
Blinnikov, S. I., Eastman, R., Bartunov, O. S., Popolitov, V. A., & Woosley, S. E. 1998, ApJ, 496, 454
Brown, P. J., Immler, S., & Swift Satellite Team. 2008, The Astronomer's Telegram, 1403, 1
Bufano, F., Pignata, G., Bersten, M., et al. 2014, MNRAS
Chu, J., Li, W., Filippenko, A. V., Blondin, S., & Narayan, G. 2008, Central Bureau Electronic Telegrams, 1271, 1
Ciabattari, F., Mazzoni, E., Donati, S., et al. 2013, Central Bureau Electronic Telegrams, 3557, 1
Ciabattari, F., Mazzoni, E., Jin, Z., et al. 2011, Central Bureau Electronic Telegrams, 2827, 1
Deng, J., Qiu, Y., & Hu, J. 2001, ArXiv Astrophysics e-prints
Drescher, C., Parker, S., Brimacombe, J., et al. 2011, Central Bureau Electronic Telegrams, 2902, 1
Ensman, L. & Burrows, A. 1992, ApJ, 393, 742
Ergon, M., Jerkstrand, A., Bersten, M., et al. 2014a, In preparation
Ergon, M., Sollerman, J., Fraser, M., et al. 2014b, A&A, 562, A17
Falk, S. W. & Arnett, W. D. 1977, ApJS, 33, 515
Fox, O. D., Azalee Bostroem, K., Van Dyk, S. D., et al. 2014, ArXiv e-prints
Fraser, M., Ergon, M., Eldridge, J., et al. 2011, MNRAS, 417, 1417
Freedman, W. L., Madore, B. F., Gibson, B. K., et al. 2001, ApJ, 553, 47
Griffith, C., Cenko, S. B., Li, W., & Filippenko, A. V. 2009, Central Bureau Electronic Telegrams, 1685, 1
Hamuy, M. 2003, ApJ, 582, 905
Hamuy, M., Deng, J., Mazzali, P. A., et al. 2009, ApJ, 703, 1612
Iglesias, C. A. & Rogers, F. J. 1996, ApJ, 464, 943
Imshennik, V. S. & Popov, D. V. 1992, AZh, 69, 497
Jacques, C., Pimentel, E., & Monard, L. A. G. 2004, IAU Circ., 8418, 1
Jerkstrand, A., Fransson, C., & Kozma, C. 2011, A&A, 530, A45
Jerkstrand, A., Fransson, C., Maguire, K., et al. 2012, A&A, 546, A28
Kelson, D. D., Illingworth, G. D., Tonry, J. L., et al. 2000, ApJ, 529, 768
Kumar, B., Pandey, S. B., Sahu, D. K., et al. 2013, MNRAS, 431, 308
Litvinova, I. I. & Nadezhin, D. K. 1983, Ap&SS, 89, 89
Litvinova, I. Y. & Nadezhin, D. K. 1985, Soviet Astronomy Letters, 11, 145
Lucy, L. B. 1999, A&A, 345, 211
Lyman, J., Bersier, D., James, P., et al. 2014, ArXiv e-prints
Maguire, K., Jerkstrand, A., Smartt, S. J., et al. 2012, MNRAS, 420, 3451
Marples, P., Parker, S., Stritzinger, M., Drescher, C., & Bock, G. 2011, Central Bureau Electronic Telegrams, 2777, 1
Maund, J. R., Smartt, S. J., Kudritzki, R. P., Podsiadlowski, P., & Gilmore, G. F. 2004, Nature, 427, 129
Mazzali, P. A. 2000, A&A, 363, 705
Mazzali, P. A., Deng, J., Hamuy, M., & Nomoto, K. 2009, ApJ, 703, 1624
Mazzali, P. A. & Lucy, L. B. 1993, A&A, 279, 447
Milisavljevic, D., Margutti, R., Soderberg, A. M., et al. 2013, ApJ, 767, 71
Monard, L. A. G. 2005, Central Bureau Electronic Telegrams, 106, 1
Monard, L. A. G. 2006a, Central Bureau Electronic Telegrams, 443, 1
Monard, L. A. G. 2006b, Central Bureau Electronic Telegrams, 385, 1
Morales-Garoffolo, A., Elias-Rosa, N., Benetti, S., et al. 2014, ArXiv e-prints
Mueller, E., Fryxell, B., & Arnett, D. 1991, A&A, 251, 505

Munari, U. & Zwitter, T. 1997, A&A, 318, 269
Nakano, S., Aoki, M., Garnavich, P., Kirshner, R., & Berlind, P. 1996, IAU Circ., 6524, 1
Nomoto, K. & Hashimoto, M. 1988, Phys. Rep., 163, 13
Paxton, B., Bildsten, L., Dotter, A., et al. 2011, ApJS, 192, 3
Pignata, G., Maza, J., Hamuy, M., et al. 2009, Central Bureau Electronic Telegrams, 1663, 1
Poznanski, D. 2013, MNRAS, 436, 3224
Poznanski, D., Prochaska, J. X., & Bloom, J. S. 2012, MNRAS, 426, 1465
Pugh, H., Park, S., & Li, W. 2004, IAU Circ., 8425, 1
Qiao, Q., Li, W., Qiu, Y., et al. 1996, IAU Circ., 6527, 1
Qiu, Y., Li, W., Qiao, Q., & Hu, J. 1999, AJ, 117, 736
Richmond, M. W., Treffers, R. R., Filippenko, A. V., & Paik, Y. 1996, AJ, 112, 732
Richmond, M. W., Treffers, R. R., Filippenko, A. V., et al. 1994, AJ, 107, 1022
Schlafly, E. F. & Finkbeiner, D. P. 2011, ApJ, 737, 103
Schlegel, D. J., Finkbeiner, D. P., & Davis, M. 1998, ApJ, 500, 525
Shigeyama, T., Suzuki, T., Kumagai, S., et al. 1994, ApJ, 420, 341
Shimasaki, K., Li, W., Yamaoka, H., & Itagaki, K. 2004, IAU Circ., 8422, 2
Taddia, M., Stritzinger, M., & Ergon, M. 2014, In preparation
Takáts, K. & Vinkó, J. 2012, MNRAS, 419, 2783
Taubenberger, S., Navasardyan, H., Maurer, J. I., et al. 2011, MNRAS, 413, 2140
Tsvetkov, D. Y., Volkov, I. M., Baklanov, P., Blinnikov, S., & Tuchin, O. 2009, Peremennye Zvezdy, 29, 2
Turatto, M., Benetti, S., & Cappellaro, E. 2003
Van Dyk, S. D., Zheng, W., Fox, O. D., et al. 2014, AJ, 147, 37
Von Neumann, J. & Richtmyer, R. D. 1950, Appl. Phys., 21, 232
Wood-Vasey, W. M., Aldering, G., Nugent, P., & Chassagne, R. 2003, IAU Circ., 8082, 1
Woosley, S. E., Eastman, R. G., Weaver, T. A., & Pinto, P. A. 1994, ApJ, 429, 300